

Optical study of the charge dynamics evolution in the topological insulators MnBi_2Te_4 and $\text{Mn}(\text{Bi}_{0.74}\text{Sb}_{0.26})_2\text{Te}_4$ under high pressure

Matthias Köpf, S. H. Lee, Z. Q. Mao, Christine A. Kuntscher

Angaben zur Veröffentlichung / Publication details:

Köpf, Matthias, S. H. Lee, Z. Q. Mao, and Christine A. Kuntscher. 2024. "Optical study of the charge dynamics evolution in the topological insulators MnBi_2Te_4 and $\text{Mn}(\text{Bi}_{0.74}\text{Sb}_{0.26})_2\text{Te}_4$ under high pressure." *Physical Review B* 109 (24): 245124. <https://doi.org/10.1103/physrevb.109.245124>.

Nutzungsbedingungen / Terms of use:

licgercopyright

Dieses Dokument wird unter folgenden Bedingungen zur Verfügung gestellt: / This document is made available under these conditions:

Deutsches Urheberrecht

Weitere Informationen finden Sie unter: / For more information see:

<https://www.uni-augsburg.de/de/organisation/bibliothek/publizieren-zitieren-archivieren/publiz/>



Optical study of the charge dynamics evolution in the topological insulators MnBi_2Te_4 and $\text{Mn}(\text{Bi}_{0.74}\text{Sb}_{0.26})_2\text{Te}_4$ under high pressure

M. Köpf¹, S. H. Lee,^{2,3} Z. Q. Mao,^{2,3,4} and C. A. Kuntscher^{1,*}

¹*Experimentalphysik II, Institute of Physics, Augsburg University, 86159 Augsburg, Germany*

²*2D Crystal Consortium, Materials Research Institute, Pennsylvania State University, University Park, Pennsylvania 16802, USA*

³*Department of Physics, Pennsylvania State University, University Park, Pennsylvania 16802, USA*

⁴*Department of Materials Science and Engineering, Pennsylvania State University, University Park, Pennsylvania 16802, USA*



(Received 9 January 2024; revised 17 May 2024; accepted 23 May 2024; published 18 June 2024)

The van der Waals material MnBi_2Te_4 and the related Sb-substituted compounds $\text{Mn}(\text{Bi}_{1-x}\text{Sb}_x)_2\text{Te}_4$ are prominent members of the family of magnetic topological insulators, in which rare quantum mechanical states can be realized. In this work, we study the evolution of the charge dynamics in MnBi_2Te_4 and the Sb-substituted compound $\text{Mn}(\text{Bi}_{1-x}\text{Sb}_x)_2\text{Te}_4$ with $x = 0.26$ under hydrostatic pressure. For MnBi_2Te_4 , the pressure dependence of the screened plasma frequency, the dc conductivity, and the reflectance at selected frequencies show weak anomalies at ~ 2 and ~ 4 GPa, which might be related to an electronic phase transition driven by the enhanced interlayer interaction. We observe a pressure-induced decrease in the optical gap, consistent with the decrease in and closing of the energy gap reported in the literature. Both studied materials show an unusual decrease in the low-energy optical conductivity under pressure, which we attribute to the decreasing spectral weight of the Drude terms describing the free charge carrier excitations. Our results suggest a localization of conduction electrons under pressure, possibly due to hybridization effects.

DOI: [10.1103/PhysRevB.109.245124](https://doi.org/10.1103/PhysRevB.109.245124)

I. INTRODUCTION

In recent years, the famous representative of topological insulators with magnetic order, MnBi_2Te_4 (MBT), has been studied extensively with many different experimental techniques. It is now proven that MBT is a promising candidate for hosting rare quantum mechanical effects such as the quantum anomalous Hall effect and the axion insulator, which makes MBT potentially interesting for applications in quantum metrology and spintronics [1–6]. Characteristic for a topological insulator, MBT exhibits a gapped electronic structure near the Fermi energy E_F in the bulk, while linearly dispersing, gapless surface states are induced by band inversion, which is protected by spatial and time-reversal symmetries at ambient conditions [7–13]. However, whether the surface states are gapped or not has been a matter of controversy, as contradictory experimental results have been reported [14,15]. Due to the onset of A-type antiferromagnetic ordering below $T_N = 25$ K [9,16–20], a time-reversal symmetry-broken system coexisting with nontrivial band topology emerges in MBT, which enables the realization of Weyl fermions close to E_F [16,21–24].

MBT crystallizes in the space group $R\bar{3}m$ with the unit cell parameters $a = 4.33$ Å and $c = 40.91$ Å [16], and it possesses a van der Waals-type layered structure, consisting of Te-Bi-Te-Mn-Te-Bi-Te septuples stacked in a rhombohedral ABC order [16,19,25]. A sketch of the structure is shown in Fig. 1(a). While the Mn sublattice contributes a

magnetic moment to the compound, the Bi and Te p_z bands are responsible for the nontrivial surface states, which are located at the Γ point in momentum space [14,26]. Regarding the three-dimensional properties, a bulk energy gap between 180 and 220 meV has been reported [8,9], while the surface Dirac point between the valence and conduction bands is located ~ 270 meV below E_F [7,9,12]. A sketch of the described band structure is shown in Fig. 2(c), where two electronic bands cross E_F . Accordingly, MBT is intrinsically doped, with electrons being the main charge carriers [21,27].

To further understand how to achieve ideal Weyl semimetal states, different methods of tuning the electronic structure in MBT have been exploited [21,28]. By gradually exchanging Bi atoms with Sb atoms, the Sb-substituted compounds $\text{Mn}(\text{Bi}_{1-x}\text{Sb}_x)_2\text{Te}_4$ (MBST) are generated, in which the position of the chemical potential and the energy gap size are strongly affected and determined by the Sb content [8,21,27,29,30]. While the structural parameters undergo only minor changes due to Sb doping, a lowering of the E_F level from the conduction bands towards the valence bands with increasing Sb content can be observed, and a nearly insulating state is expected to be reached at a doping level of $x = 0.26$ [8,21]. Accordingly, the expected electronic band structure of $\text{Mn}(\text{Bi}_{0.74}\text{Sb}_{0.26})_2\text{Te}_4$ ($x = 0.26$) is sketched in Fig. 2(f), where E_F now slightly crosses one of the lower bands, as will be justified later based on our experimental results. In addition, the energy gap is reported to be reduced with Sb doping level, where a gap closing is expected at $x = 0.55$, and a reopening of the bands results in the vanishing of nontrivial bands for Sb-substituted compounds above $x = 0.55$ [8].

*Contact author: christine.kuntscher@physik.uni-augsburg.de

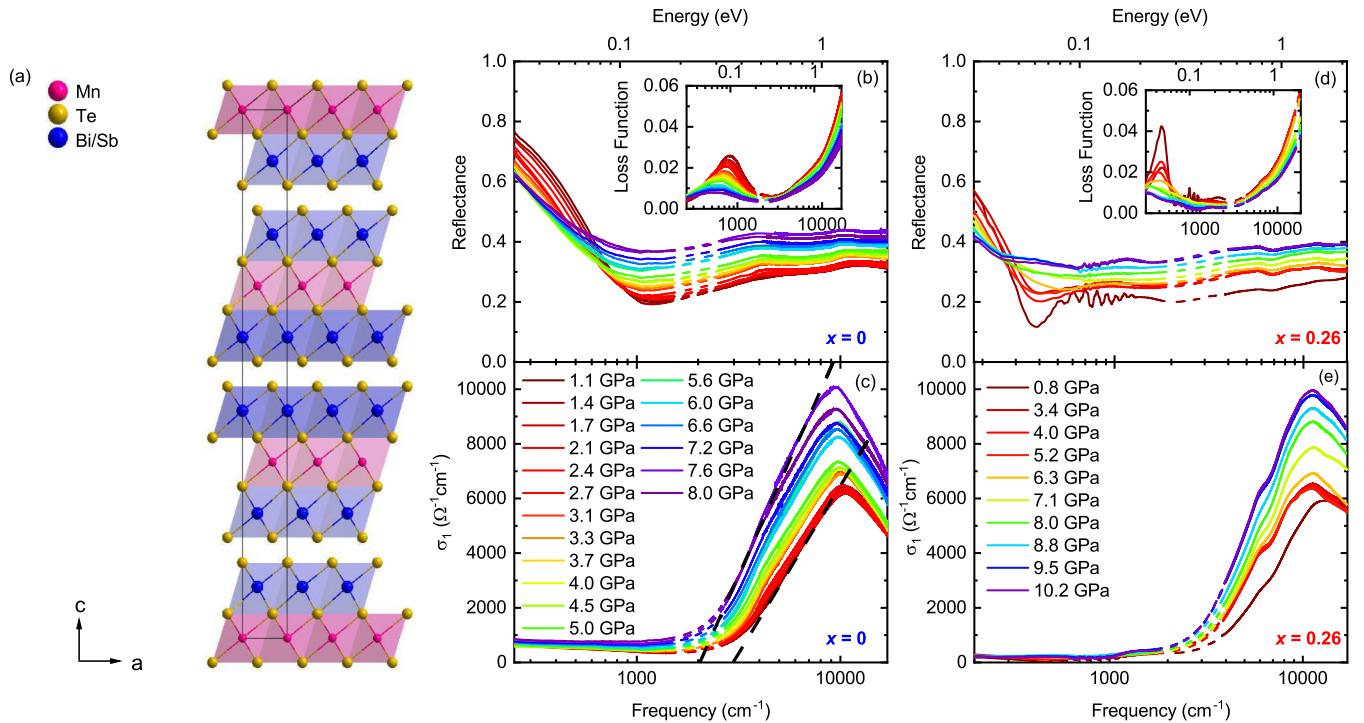


FIG. 1. (a) Sketch of the crystal structure of MBST. Pressure-dependent (b) reflectance and (c) optical conductivity σ_1 of the pure compound and (d) reflectance and (e) optical conductivity σ_1 of the Sb-substituted compound with $x = 0.26$. The corresponding loss functions of both materials are shown in the insets in (b) and (d), respectively. In (c), the intercept point of the linear extrapolations (dashed lines) of σ_1 with the frequency axis indicates the onset of interband transitions, corresponding to the optical gap size.

However, topological surface states have also been detected in MnSb_2Te_4 ($x = 1$) in other studies [31–34].

Thus far, the optical properties of pure MBT and of various Sb-substituted compounds MBST have been investigated only at ambient pressure [35–38]. As unusual properties of pressurized MBT with regard to dc electric transport dynamics, electronic structure, and structural evolution have been reported [39–44], it is important to also investigate the frequency-dependent optical response of MBT at high hydrostatic pressures. Typically, materials show a decreasing resistivity under external pressure, as bond lengths and interatomic distances are more and more compressed [45]. This holds, for example, for the closely related compounds and topological insulators Bi_2Te_3 [46] and MnSb_2Te_4 [47]. In stark contrast, several studies revealed a more complex behavior of the dc resistivity for MBT under hydrostatic pressure [39,41]. Electrical resistivity measurements show the initial *increase* in resistivity with increasing pressure up to ~ 12 GPa, followed by a strong resistivity drop for higher pressures. This unconventional, nonmonotonic shift was suggested to result from the competing nature of gradually localized surface electrons and the bulk electrons undergoing a delocalization process under pressure [39]. In another study, the hybridization of Bi $6p$ and Te $5p$ electrons with delocalized Mn $3d$ electrons, which creates a hybridization gap, and an increase in electron scattering rate were given as possible mechanisms for the initial pressure-induced resistivity increase [41]. Regarding the crystal structure under pressure, the cell parameters a and c shrink irregularly with increasing pressure [41]. This results in an unusual evolution in the c/a ratio, where an initial drop to a minimum value at 3 GPa is followed

by an increase for higher pressures [39]. A further crucial consequence of external pressure application is a decrease in the energy gap at the Γ point up to ~ 15 GPa [39,42], as demonstrated by various theoretical calculations [39,40,42]. In summary, the high-pressure properties of MBT are highly unusual, and many open questions remain.

In this study, we investigate the effect of external pressure on the charge carrier dynamics in pure MBT and in the Sb-substituted compound $\text{Mn}(\text{Bi}_{0.74}\text{Sb}_{0.26})_2\text{Te}_4$ using optical spectroscopy over a broad frequency range. According to our optical data, the metallic character of both compounds weakens under pressure. We also find anomalies in the pressure dependence of the screened plasma frequency $\omega_{\text{pl}}^{\text{scr}}$, dc conductivity, and reflectance values at selected frequencies. These pressure-induced anomalies are in good agreement with the structural parameter evolutions under pressure reported in the literature [39,41]. Furthermore, we observe a decrease in the optical gap, which we relate to the decreasing energy gap under pressure [39,42].

II. MATERIALS AND METHODS

Single crystals of MnBi_2Te_4 and $\text{MnBi}_{(0.74}\text{Sb}_{0.26)}_2\text{Te}_4$ were grown by the self-flux method as reported in Ref. [21]. The 26% Sb-substituted sample belongs to batch SL3B1 described in our previous publication [38], and, accordingly, is slightly hole doped. The crystals were characterized in detail by temperature-dependent electric transport and Hall resistivity measurements, as reported in Ref. [21]. We carried out infrared reflectance measurements by Fourier-transform

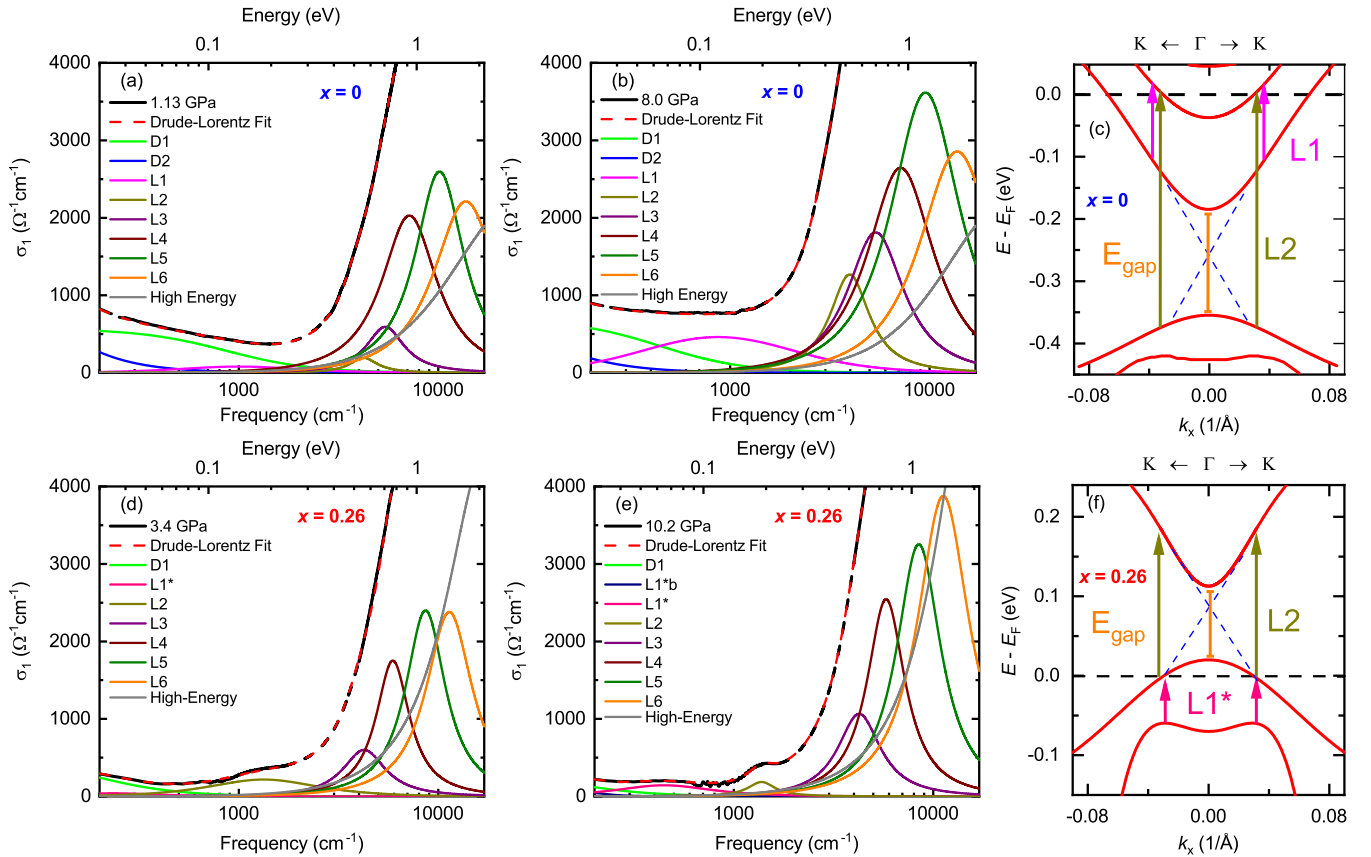


FIG. 2. Drude-Lorentz fit of σ_1 of the pure compound at (a) 1.13 GPa and (b) 8.0 GPa and of the 26% substituted compound at (d) 3.4 GPa and (e) 10.2 GPa. (c) and (f) display sketches of the corresponding band structures close to the Fermi level (similar to Ref. [38] and based on calculations by Chen *et al.* [9]). In (c) and (f), the vertical arrows display electronic transitions described by the respective Lorentz oscillators, where L1 describes transitions between two conduction bands, L1* describes transitions between the valence and conduction bands, and L2 corresponds to transitions across the optical gap. The energy gap E_{gap} is indicated by a vertical orange line.

infrared spectroscopy with a Bruker 80v spectrometer coupled to a Hyperion microscope.

Hydrostatic pressure was applied with EasyLab diamond anvil cells (DACs), where a small piece of the single crystal was placed into a hole of a CuBe gasket together with some CsI, which served as the pressure-transmitting medium for the realization of quasi-hydrostatic pressure. For the pure compound we used a DAC with a 900 μm culet size, and for the 26% substituted sample a DAC with a 800 μm culet size was selected. In order to determine the pressure inside the DAC, tiny Al_2O_3 spheres were placed next to the sample. Excited with a green laser, these spheres emit radiation with a specific wavelength characteristic of the applied pressure. This radiation was detected with a charge-coupled device spectrograph.

The reflectance was calculated according to the equation $I_{\text{sample}}/I_{\text{reference}}$, where I_{sample} stands for the intensity reflected by the sample and $I_{\text{reference}}$ stands for the intensity reflected by the CuBe gasket. The data were measured from ~ 200 to $17\,000\text{ cm}^{-1}$ (0.03 to 2.11 eV). Over a small range from ~ 1700 to 2700 cm^{-1} , the measured spectra had to be interpolated, as the characteristic multiphonon absorption in diamond led to false results [48]. Also, extrapolations in the low- and high-energy regimes are merged with the spectra. These extrapolations are constructed with the help of literature values from transport measurements and volumetric

information, which is necessary to obtain optical functions, like the optical conductivity σ_1 and the loss function $-\text{Im}(1/\epsilon)$. This is done by applying the Kramers-Kronig relations through programs by Tanner [49]. All datasets are fitted with the Drude-Lorentz model to learn about the pressure-dependent behavior of various electronic excitations with the use of the REFFIT software, as described by Kuzmenko [50].

III. RESULTS

A. Pressure-dependent optical spectra

The room-temperature reflectance spectra of MBT as a function of pressure were measured in small steps up to 8.0 GPa. In order to establish a good sample-diamond interface, which is necessary for reasonable results, the first spectrum was taken at 1.1 GPa. The results are shown in Fig. 1(b). At the lowest pressure, we find a characteristic metallic spectrum: The reflectivity level at the lowest measured frequency is quite high, close to 80%, which is followed by a rather strong decrease corresponding to the plasma edge. The reflectance shows the plasma minimum at $\sim 1200\text{ cm}^{-1}$ and a weak but steady increase up to the highest measured frequency. With increasing pressure, this profile is maintained. However, we observe that the level below $\sim 700\text{ cm}^{-1}$ decreases with increasing pressure, while above

this wave number a reflectance increase is found. The corresponding optical conductivity spectra [see Fig. 1(c)] show, for all measured pressures, a low level ($\sim 1000 \Omega^{-1} \text{cm}^{-1}$) at low frequencies, which is followed by a linearlike increase above $\sim 2000 \text{cm}^{-1}$. This quasilinear increase in σ_1 has been extrapolated with linear fits in order to estimate the size of the optical gap, as will be discussed later. The high-frequency range is dominated by a pronounced absorption band centered at around $10\,000 \text{cm}^{-1}$ due to interband transitions, which is in good agreement with previous measurements by our group [36–38] and by Xu *et al.* [35]. With increasing pressure this absorption band increases in strength and shifts slightly to smaller frequencies. The inset in Fig. 1(b) shows the loss function of MBT as a function of pressure, defined as $-\text{Im}(1/\hat{\epsilon})$, where $\hat{\epsilon}$ is the complex dielectric function. A clear plasmon peak in the loss function at the lowest pressure indicates the metallic character of the material, and its position corresponds to the value of the screened plasma frequency $\omega_{\text{pl}}^{\text{scr}}$. With increasing pressure the plasmon peak shifts from $\sim 800 \text{cm}^{-1}$ at 1.1 GPa to lower frequencies and broadens considerably, both signaling a weakening of the metallic character of MBT under pressure, as will be discussed below.

Corresponding optical functions of the 26 % Sb-doped compound are displayed in Figs. 1(d) and 1(e) at various pressures up to 10.2 GPa. The overall pressure dependence of the optical response is very similar to that of the undoped material MBT. However, the metallic character of $\text{Mn}(\text{Bi}_{0.74}\text{Sb}_{0.26})_2\text{Te}_4$ is much more reduced compared to MBT: Namely, the low-frequency reflectivity level is low, and the plasma edge is less developed with a plasma minimum located at a lower frequency [$\sim 400 \text{cm}^{-1}$; see Fig. 1(d)]. Also the Fabry-Pérot interferences in the frequency range $500\text{--}1300 \text{cm}^{-1}$ signal the much reduced metallic nature, leading to a partial transparency of the studied crystal. The Fabry-Pérot interferences are reduced under pressure. At higher frequencies, the level of the reflectivity rises very weakly, similar to the pure compound [see Fig. 1(b)]. The low-frequency optical conductivity σ_1 , depicted in Fig. 1(e), has an extremely low level up to frequency 1000cm^{-1} , confirming the very low spectral weight of free charge carrier excitations. As expected, the material is close to insulating. A small plateau-like feature in σ_1 at $\sim 1500 \text{cm}^{-1}$ is followed by a steep quasilinear increase to high values and an absorption band due to interband transitions. The plasmon peak in the loss function of $\text{Mn}(\text{Bi}_{0.74}\text{Sb}_{0.26})_2\text{Te}_4$ [see inset of Fig. 1(d)] indicates the pressure-induced weakening of the (already weak) metallic character like for MBT, namely, a decrease of its height, broadening, and a shift to lower frequencies.

B. Analysis of optical functions and optical parameters as a function of pressure

For a detailed understanding of the charge carrier dynamics and excitations under pressure, we performed fits of the measured optical data with the Drude-Lorentz model. Fits of the optical conductivity σ_1 of MBT at the lowest and highest pressures are depicted in Figs. 2(a) and 2(b), respectively. As free charge carrier contributions from two electronic bands are expected according to the electronic band structure of MBT [Fig. 2(c)] and in order to obtain a reasonable fit of the

data, we have implemented two Drude terms in addition to six Lorentz terms in the measured range. This fit model is in accordance with previous analyses by our group [36,38]. The “High-Energy” oscillator stands for the sum of all oscillators lying outside the measured range. From the comparison of the Drude contributions at the lowest and highest measured pressures, we can conclude that the Drude terms lose spectral weight under pressure, whereas all the Lorentz oscillators gain in spectral weight. The electronic band structure of MBT sketched in Fig. 2(c) is based on calculations by Chen *et al.* [9] and was already discussed in Refs. [36,38]. The two energetically lowest interband transitions, L1 and L2, correspond to transitions between the two conduction bands and to the lowest-energy transitions between the valence and conduction bands, defining the optical gap, respectively. Especially, L1 increases a lot in oscillator strength when the external pressure is increased, which lifts the level of σ_1 around 1000cm^{-1} .

For the 26% substituted compound $\text{Mn}(\text{Bi}_{0.74}\text{Sb}_{0.26})_2\text{Te}_4$, the behavior of the optical conductivity under pressure is partially similar. Comparing the data shown in Fig. 2 at 3.4 GPa [Fig. 2(d)] and at 10.2 GPa [Fig. 2(e)], the Lorentz oscillators in the high-energy range gain in spectral weight. The initial excitation resulting from interband transitions, also referred to as the optical gap, is described by the L2 oscillator, which is located just below the quasilinear increase. This peak undergoes a slight shift to lower frequencies as well as a narrowing under pressure. The spectral weight of σ_1 below $\sim 1000 \text{cm}^{-1}$ has a very low level, with a pressure-induced decrease in the Drude spectral weights and an increase in the L1* oscillator strength. L1* describes the electronic transitions between the valence and conduction bands, as illustrated in Fig. 2(f). Compared to those of MBT, in $\text{Mn}(\text{Bi}_{0.74}\text{Sb}_{0.26})_2\text{Te}_4$ the energy gap E_{gap} is reduced, and the Fermi level is shifted down in energy and is expected to slightly cut one of the former valence bands [8]. Also, we observe an additional oscillator L1*b located at around 200cm^{-1} which appears for pressures above 8.8 GPa. This weak excitation seems to be less screened with increasing pressure, as the spectral weight of the Drude contributions and the overall σ_1 level are reduced. To conclude, both samples from this compound family show similar pressure dependences, in particular, a strong reduction of the Drude spectral weights under pressure.

The pressure evolution of several optical parameters is depicted in Fig. 3, highlighting the most important findings of our study. In Fig. 3(a) we show the reflectance values for MBT at selected frequencies below 1000cm^{-1} as a function of pressure. We observe two weak anomalies in the pressure dependence at around 2 and 4.5 GPa which signal abrupt changes in the electronic properties under pressure. The pressure-dependent value of the dc conductivity σ_{dc} of MBT as extracted from the Drude-Lorentz fits is depicted in Fig. 3(b). Obviously, σ_{dc} undergoes a strong decrease from $\sim 2500 \Omega^{-1} \text{cm}^{-1}$ at 1 GPa to $1600 \Omega^{-1} \text{cm}^{-1}$ at 4 GPa, followed by a constant behavior. We compare our experimental data to results from Pei *et al.* [39] measured at room temperature and from Chen *et al.* [41] measured on two samples at 250 and 200 K. In addition to the difference in absolute values, we observe different slopes in the pressure dependence of σ_{dc} compared to our data. Yet in all cases the dc conductivity decreases with increasing external pressure. A small

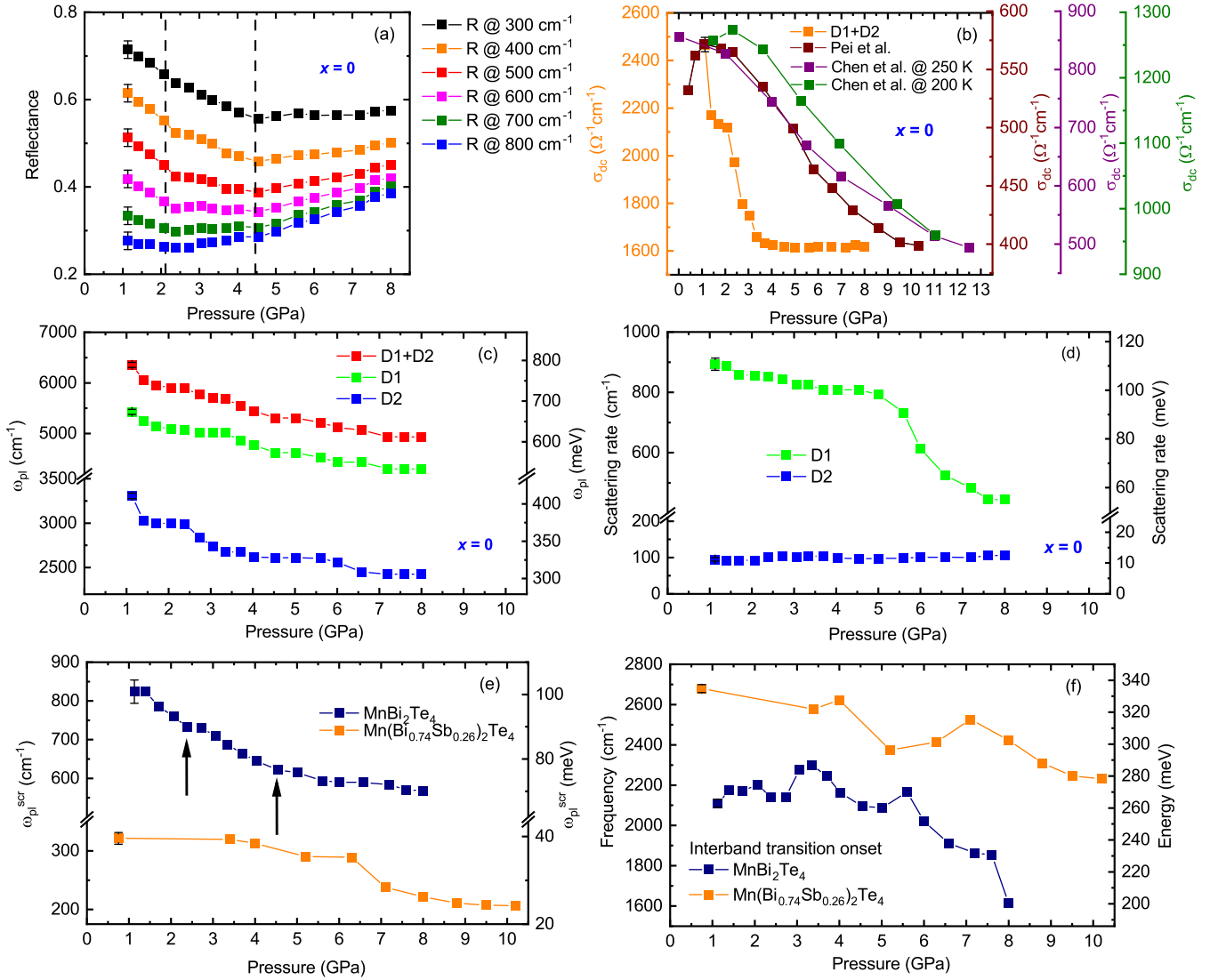


FIG. 3. (a) Reflectance values of MBT at selected frequencies as a function of pressure. The dashed vertical lines highlight the anomalies at ~ 2 and ~ 4 GPa. (b) σ_{dc} values of MBT obtained with the Drude-Lorentz fits, which are compared to results from Pei *et al.* [39] and Chen *et al.* [41]. (c) Plasma frequency ω_{pl} of the two Drude terms, D1 and D2, and the total plasma frequency of the combination D1+D2 (see text for definition) for MBT as a function of pressure. (d) Scattering rate of Drude terms D1 and D2 for MBT as a function of pressure. (e) Screened plasma frequency ω_{pl}^{scr} of the pure and the 26% doped samples, as obtained from the plasmon peak position in the loss function. Two anomalies in the pressure dependence of ω_{pl}^{scr} for MBT at ~ 2 and ~ 4 GPa are indicated by vertical arrows. (f) Interband transition onset for MBT and the $x = 0.26$ doped sample as a function of pressure, determined by the zero crossing of the linear extrapolations in the σ_1 spectra, which is an estimate for the size of the optical gap. The error bars in (a) have been estimated within the accuracy of the reflection measurement.

pressure-induced increase of the dc conductivity at pressures below 3 GPa was observed by Pei *et al.* [39] and for a sample at 200 K by Chen *et al.* [41], which was followed by a strong decrease above. This initial discrepancy is not visible in our data, where σ_{dc} decreases already from the lowest pressure onwards.

As a measure of the metallic character of a material we can furthermore consider the plasma frequency, which corresponds to the Drude spectral weight, and the scattering rate of the Drude terms, as extracted from the Drude-Lorentz fits. In Fig. 3(c) the values of ω_{pl} of Drude terms D1 ($\omega_{pl,1}$) and D2 ($\omega_{pl,2}$) and the total plasma frequency, labeled “D1+D2” and calculated according to $\omega_{pl} = \sqrt{\omega_{pl,1}^2 + \omega_{pl,2}^2}$, are shown

as a function of pressure. The value of ω_{pl} (as well as of $\omega_{pl,1}$ and $\omega_{pl,2}$) decreases under pressure, clearly indicating the weakening of the metallic character. The scattering rate of Drude term D1 [see Fig. 3(d)] shows a small decrease up to 5 GPa, followed by a stronger drop at higher pressures. The scattering rate of D2 is approximately pressure independent.

Another characterization of the free charge carrier dynamics is given by the screened plasma frequency ω_{pl}^{scr} , which can be obtained from the plasmon peak position in the loss function [see insets in Figs. 1(b) and 1(d)]. ω_{pl}^{scr} is related to the plasma frequency ω_{pl} according to $\omega_{pl}^{scr} = \omega_{pl} / \sqrt{\epsilon_{\infty}}$, where ϵ_{∞} is the high-frequency value of $\epsilon_1(\omega)$. For the MBT compound ω_{pl}^{scr} decreases under pressure, with weak

anomalies at ~ 2 and ~ 4.5 GPa indicated by arrows in Fig. 3(e). Like for the pressure-dependent reflectance values, these anomalies signal abrupt changes in the electronic structure. For $\text{Mn}(\text{Bi}_{0.74}\text{Sb}_{0.26})_2\text{Te}_4$ the value of $\omega_{\text{pl}}^{\text{scr}}$ also decreases under pressure. To conclude, the unscreened and screened plasma frequencies are reduced under pressure for both studied materials, indicating that they become less metallic for pressures up to ~ 10 GPa, in good agreement with published dc transport experiments [39,41]. Such pressure behavior is very unusual since the overlap of atomic orbitals generally increases under pressure, which leads to an increase in electronic band width and hence improved conductivity.

A further important parameter characterizing the electronic band structure is the size of the optical gap. In order to extract the optical gap size from our data, we extrapolated the quasilinear increase in σ_1 with a linear extrapolation, as mentioned above and as sketched in Fig. 1(c). The zero crossing of this extrapolation marks the onset of the interband transitions and hence is an estimate of the size of the optical gap. The so-obtained values of the interband transition onset as a function of pressure are plotted in Fig. 3(f) for the pure and 26% substituted compounds. For MBT we observe an approximately constant value of 2200 cm^{-1} up to ~ 6 GPa, followed by a drop to 1600 cm^{-1} at 8 GPa. In the case of $\text{Mn}(\text{Bi}_{0.74}\text{Sb}_{0.26})_2\text{Te}_4$ the interband transition onset decreases from 2700 to 2200 cm^{-1} . Accordingly, in both materials the optical gap is reduced under pressure.

IV. DISCUSSION

A. Pressure-induced anomalies in the optical data

For MBT, we observe weak anomalies at ~ 2 and ~ 4 GPa in the pressure dependence of the reflectance at selected frequencies [Fig. 3(a)], the dc conductivity σ_{dc} [Fig. 3(b)], and the screened plasma frequency $\omega_{\text{pl}}^{\text{scr}}$ [Fig. 3(e)], suggesting abrupt changes in the electronic band structure. These changes could be interrelated to abrupt pressure-induced changes in the crystal structure reported in the literature. Chen *et al.* [41] observed a sudden drop in the pressure dependence of the lattice parameters a and c at 2 GPa, which was interpreted in terms of a lattice softening. According to experimental and theoretical results in Refs. [39,42], respectively, the interlayer lattice parameter c is more sensitive to pressure than the intralayer lattice parameter a for low pressures up to ~ 2 GPa. However, this behavior changes for higher pressures, namely, above ~ 4 GPa, since the interlayer distance is less affected in this pressure range. Accordingly, the lattice parameter ratio c/a initially decreases under pressure and exhibits a minimum between ~ 2 and ~ 4 GPa, followed by an almost linear increase above 4 GPa up to ~ 14 GPa [39]. The pressure dependence of the c/a ratio can be related to anomalies in the pressure shift of several structural parameters [39]: For example, various bond distances between the Mn, Bi, and Te atoms, like the Mn-Te and Bi-Te bond lengths, decrease under pressure, with anomalous behavior between 2 and 4 GPa. Such pressure dependence is also revealed by the Te-Te bond length, which is a measure for the interlayer distance, and by the bond angles within the Te-Bi-Te octahedra. In addition, the intensity ratio of the strongest Raman-active modes follows

this anomalous pressure dependence. It is important to note that no crystal symmetry change occurs for pressures below 14.6 GPa [39].

Interestingly, in the closely related compounds Bi_2Te_3 , Bi_2Se_3 , and Sb_2Te_3 a Lifshitz transition [51], i.e., an electronic topological transition with changes in the Fermi surface topology *without* a lattice symmetry change, has been reported to occur between 3 and 5 GPa [52–55]. The layered, polar semiconductor BiTeI, which turns into a topological insulator under moderate pressure [56], is another example where an electronic topological transition has been observed between 2 and 3 GPa [57]: The pressure evolution of the c/a lattice parameter ratio has a minimum in the absence of lattice symmetry change, and the optical parameters show anomalous behavior, similar to our findings for MBT. Layered compounds are generally prone to pressure-induced electronic topological transitions [58–60], as also evidenced in BiTeBr [61], 1T-TiTe₂ [62], and ZrSiTe [63,64]. A topological phase transition has, indeed, been theoretically predicted for MBT under hydrostatic tensile strain [40] and suggested to occur in pressurized MBT [39] and in the doping series $(\text{Mn}_{1-x}\text{Pb}_x)\text{Bi}_2\text{Te}_4$ [65]. The closely related material MnSb_2Te_4 undergoes a pressure-induced topological phase transition when the interlayer distance is decreased by a critical percentage [66]. Interlayer interaction therefore seems to be the driving mechanism for this phase transition. Considering the anomalous behavior of the c/a ratio in MBT under pressure as described above, a similar scenario might hold here as well. The occurrence of a Lifshitz transition in pressurized MBT due to an enhanced interlayer interaction thus seems very likely.

In the case of $\text{Mn}(\text{Bi}_{0.74}\text{Sb}_{0.26})_2\text{Te}_4$ we cannot draw a conclusion regarding anomalies in the low-energy optical response since this compound is less metallic (in fact, close to insulating) and therefore the pressure-induced changes are much less developed.

B. Optical gap evolution

The energy gap evolution might also be linked to these pressure-induced structural anomalies. Based on theoretical calculations, Xu *et al.* [42] found a slight increase in the energy gap in MBT up to ~ 2 GPa, followed by an almost linear decrease and a gap closing slightly above 15 GPa. We cannot directly extract the energy gap from our optical data since it is smaller than the optical gap, i.e., the onset of interband transitions [see the energy scheme in Fig. 2(c)]. The size of the optical gap can serve only as an upper bound for the energy gap size. According to our optical results presented in Fig. 3(e), the optical gap decreases with increasing pressure for both studied compounds.

C. Charge carrier dynamics under pressure

The weakening of the metallic character of MBT under pressure is puzzling, and possible reasons for it have been discussed in the literature. Pei *et al.* [39] ascribed the pressure-induced increase in resistivity to the competition between the localization of the surface electrons and the delocalization of the bulk electrons, where the first process is predominant in

the pressure range between 3 and ~ 15 GPa, resulting in a resistivity increase. Such a resistivity increase, i.e., decrease in metallic character, is consistent with our optical results. However, our optical data do not confirm the proposed scenario: Since infrared spectroscopy is generally bulk sensitive with only minor contributions from surface electrons, the observed pressure-induced decrease in conductivity is a bulk property according to our optical results.

Based on Hall effect measurements, Chen *et al.* [41] related the pressure-induced increase in resistivity to a decrease in electron mobility μ_e , despite the observed increase in charge carrier density n_e under pressure. Two scenarios were discussed as possible explanations [41]. In the first scenario, the pressure-induced suppression of long-range antiferromagnetic order in MBT causes an enhancement of magnetic fluctuations, which increases the electron scattering. The electron scattering rate γ is related to the mobility μ_e according to

$$\mu_e = \frac{e}{m_e^* \gamma}, \quad (1)$$

where m_e^* denotes the effective electron mass [67,68]. Accordingly, an enhanced scattering rate would cause a decrease in μ_e and hence a localization of charge carriers with an enhancement of the resistivity. Since the carrier scattering determines the width of the Drude terms in our optical conductivity data, we can test this scenario. As shown in Fig. 3(d) the scattering rate of the dominant Drude term, D1, decreases with increasing pressure, with a stronger drop above ~ 5 GPa. Interestingly, above this pressure the suppression of the antiferromagnetic ordering occurs [39,41]. For the weaker Drude contribution, D2, the scattering rate is pressure independent. Therefore, our optical results do not support an enhancement of the scattering rate under pressure, as suggested in Ref. [41].

According to Eq. (1), the mobility of the carriers can also be affected by their effective mass: A pressure-induced increase in m_e^* would cause a decrease in μ_e consistent with the Hall effect experiments. In fact, an increase in m_e^* would also explain the pressure-induced decrease in the plasma frequency ω_{pl} [see Fig. 3(c)] since ω_{pl} depends on m_e^* according to [69]

$$\omega_{\text{pl}} = \sqrt{\frac{n_e e^2}{\epsilon_0 m_e^*}}. \quad (2)$$

Thus, an increase in m_e^* under pressure could explain both the observed decrease in carrier mobility and the decrease

in plasma frequency, despite the increase in electron density n_e [41]. A pressure-induced enhancement of the effective electron mass would be consistent with the second scenario proposed in Ref. [41]: In analogy to CaMn_2Bi_2 [70–72], pressure application could induce a partial delocalization of Mn $3d$ electrons and subsequent hybridization with Bi $6p$ and/or Te $5p$ conduction electrons, causing a localization of the electrons and the opening of a hybridization gap [41]. Our optical data are consistent with a maximum gap size of ~ 15 meV at 4 GPa. The scenario of a pressure-induced localization of charges due to hybridization could explain the results from Hall effect measurements as well as our optical data for both studied materials.

V. CONCLUSION

In this work, we studied the charge dynamics of the topological insulators MnBi_2Te_4 and $\text{Mn}(\text{Bi}_{0.74}\text{Sb}_{0.26})_2\text{Te}_4$ at high pressures by determining the optical response functions. In good agreement with other pressure studies on MnBi_2Te_4 [39–43], we detected a pressure-induced decrease in the metallic strength for both materials based on the low-energy optical response. This decrease in conductivity is possibly due to an enhanced effective mass resulting from the creation of a hybridization gap. Furthermore, several optical parameters showed weak anomalies in their pressure dependence at ~ 2 and ~ 4 GPa, which might originate from a topological electronic transition. In analogy to the closely related material MnSb_2Te_4 , we suggest the enhancement of interlayer interaction as the driving mechanism for this phase transition. In addition, we observed a pressure-induced decrease in the optical gap size for both studied materials, indirectly confirming the expected reduction of the energy gap under pressure.

ACKNOWLEDGMENTS

The authors acknowledge fruitful discussions with and technical support by J. Ebad-Allah. C.A.K. acknowledges financial support from the Deutsche Forschungsgemeinschaft (DFG), Germany, through Grant No. KU 1432/15-1. Z.Q.M. and S.H.L. acknowledge the support of the U.S. NSF through the Penn State 2D Crystal Consortium-Materials Innovation Platform (2DCC-MIP) under NSF Cooperative Agreement No. DMR-2039351.

-
- [1] S. Zhang, R. Wang, X. Wang, B. Wei, B. Chen, H. Wang, G. Shi, F. Wang, B. Jia, Y. Ouyang, F. Xie, F. Fei, M. Zhang, X. Wang, D. Wu, X. Wan, F. Song, H. Zhang, and B. Wang, Experimental observation of the gate-controlled reversal of the anomalous Hall effect in the intrinsic magnetic topological insulator MnBi_2Te_4 Device, *Nano Lett.* **20**, 709714 (2019).
- [2] Y. Deng, Y. Yu, M. Z. Shi, Z. Guo, Z. Xu, J. Wang, X. H. Chen, and Y. Zhang, Quantum anomalous Hall effect in intrinsic magnetic topological insulator MnBi_2Te_4 , *Science* **367**, 895 (2020).
- [3] C. Lei and A. H. MacDonald, Gate-tunable quantum anomalous Hall effects in MnBi_2Te_4 thin films, *Phys. Rev. Mater.* **5**, L051201 (2021).
- [4] K. He, MnBi_2Te_4 -family intrinsic magnetic topological materials, *npj Quantum Mater.* **5**, 90 (2020).
- [5] Y. Li, Z. Jiang, J. Li, S. Xu, and W. Duan, Magnetic anisotropy of the two-dimensional ferromagnetic insulator MnBi_2Te_4 , *Phys. Rev. B* **100**, 134438 (2019).
- [6] J. Li, C. Wang, Z. Zhang, B.-L. Gu, W. Duan, and Y. Xu, Magnetically controllable topological quantum phase transitions in the antiferromagnetic topological insulator MnBi_2Te_4 , *Phys. Rev. B* **100**, 121103(R) (2019).
- [7] Y. Hao, P. Liu, Y. Feng, X. Ma, E. Schwier, M. Arita, S. Kumar, C. Hu, R. Lu, M. Zeng, Y. Wang, Z. Hao, H. Sun, K. Zhang, J. Mei, N. Ni, L. Wu, K. Shimada, C. Chen, Q. Liu *et al.*, Gapless

- surface Dirac cone in antiferromagnetic topological insulator MnBi_2Te_4 , *Phys. Rev. X* **9**, 041038 (2019).
- [8] B. Chen, F. Fei, D. Zhang, B. Zhang, W. Liu, S. Zhang, P. Wang, B. Wei, Y. Zhang, Z. Zuo, J. Guo, Q. Liu, Z. Wang, X. Wu, J. Zong, X. Xie, W. Chen, Z. Sun, S. Wang, Y. Zhang *et al.*, Intrinsic magnetic topological insulator phases in the Sb doped MnBi_2Te_4 bulks and thin flakes, *Nat. Commun.* **10**, 4469 (2019).
- [9] Y. J. Chen, L. X. Xu, J. H. Li, Y. W. Li, H. Y. Wang, C. F. Zhang, H. Li, Y. Wu, A. J. Liang, C. Chen, S. W. Jung, C. Cacho, Y. H. Mao, S. Liu, M. X. Wang, Y. F. Guo, Y. Xu, Z. K. Liu, L. X. Yang, and Y. L. Chen, Topological electronic structure and its temperature evolution in antiferromagnetic topological insulator MnBi_2Te_4 , *Phys. Rev. X* **9**, 041040 (2019).
- [10] M. M. Otrokov, I. P. Rusinov, M. Blanco-Rey, M. Hoffmann, A. Y. Vyazovskaya, S. V. Ereemeev, A. Ernst, P. M. Echenique, A. Arnau, and E. V. Chulkov, Unique thickness-dependent properties of the van der Waals interlayer antiferromagnet MnBi_2Te_4 films, *Phys. Rev. Lett.* **122**, 107202 (2019).
- [11] I. I. Klimovskikh, M. M. Otrokov, D. Estyunin, S. V. Ereemeev, S. O. Filnov, A. Koroleva, E. Shevchenko, V. Voroshnin, I. P. Rusinov, M. Blanco-Rey, M. Hoffmann, Z. S. Aliev, M. B. Babanly, I. R. Amiraslanov, N. A. Abdullayev, V. N. Zverev, A. Kimura, O. E. Tereshchenko, K. A. Kokh, L. Petaccia *et al.*, Tunable 3D/2D magnetism in the $(\text{MnBi}_2\text{Te}_4)(\text{Bi}_2\text{Te}_3)_m$ topological insulators family, *npj Quantum Mater.* **5**, 54 (2020).
- [12] P. Swatek, Y. Wu, L.-L. Wang, K. Lee, B. Schrunk, J. Yan, and A. Kaminski, Gapless Dirac surface states in the antiferromagnetic topological insulator MnBi_2Te_4 , *Phys. Rev. B* **101**, 161109(R) (2020).
- [13] R. C. Vidal, H. Bentmann, T. R. F. Peixoto, A. Zeugner, S. Moser, C.-H. Min, S. Schatz, K. Kibner, M. nzelmann, C. I. Fornari, H. B. Vasili, M. Valvidares, K. Sakamoto, D. Mondal, J. Fujii, I. Vobornik, S. Jung, C. Cacho, T. K. Kim, R. J. Koch, C. Jozwiak *et al.*, Surface states and Rashba-type spin polarization in antiferromagnetic MnBi_2Te_4 (0001), *Phys. Rev. B* **100**, 121104(R) (2019).
- [14] S. H. Lee, Y. Zhu, Y. Wang, L. Miao, T. Pillsbury, H. Yi, S. Kempinger, J. Hu, C. A. Heikes, P. Quarterman, W. Ratcliff, J. A. Borchers, H. Zhang, X. Ke, D. Graf, N. Alem, C. Z. Chang, N. Samarth, and Z. Mao, Spin scattering and noncollinear spin structure-induced intrinsic anomalous Hall effect in antiferromagnetic topological insulator MnBi_2Te_4 , *Phys. Rev. Res.* **1**, 012011(R) (2019).
- [15] M. M. Otrokov, I. I. Klimovskikh, H. Bentmann, D. Estyunin, A. Zeugner, Z. S. Aliev, S. Gass, A. U. B. Wolter, A. V. Koroleva, A. M. Shikin, M. Blanco-Rey, M. Hoffmann, I. P. Rusinov, A. Yu. Vyazovskaya, S. V. Ereemeev, Yu. M. Koroteev, V. M. Kuznetsov, F. Feysel, J. Sanchez-Barriga, I. R. Amiraslanov *et al.*, Prediction and observation of an antiferromagnetic topological insulator, *Nature (London)* **576**, 416 (2019).
- [16] H. Li, S. Liu, C. Liu, J. Zhang, Y. Xu, R. Yu, Y. Wu, Y. Zhang, and S. Fan, Antiferromagnetic topological insulator MnBi_2Te_4 : Synthesis and magnetic properties, *Phys. Chem. Chem. Phys.* **22**, 556 (2020).
- [17] L. Ding, C. Hu, F. Ye, E. Feng, N. Ni, and H. Cao, Crystal and magnetic structures of magnetic topological insulators MnBi_2Te_4 and MnBi_4Te_7 , *Phys. Rev. B* **101**, 020412(R) (2020).
- [18] Y. Yuan, X. Wang, H. Li, J. Li, Y. Ji, Z. Hao, Y. Wu, K. He, Y. Wang, Y. Xu, W. Duan, W. Li, and Q.-K. Xue, Electronic states and magnetic response of MnBi_2Te_4 by scanning tunneling microscopy and spectroscopy, *Nano Lett.* **20**, 3271 (2020).
- [19] P. Rani, A. Saxena, R. Sultana, V. Nagpal, S. S. Islam, S. Patnaik, and V. P. S. Awana, Crystal growth and basic transport and magnetic properties of MnBi_2Te_4 , *J. Supercond. Novel Magn.* **32**, 3705 (2019).
- [20] J. Cui, M. Shi, H. Wang, F. Yu, T. Wu, X. Luo, J. Ying, and X. Chen, Transport properties of thin flakes of the antiferromagnetic topological insulator MnBi_2Te_4 , *Phys. Rev. B* **99**, 155125 (2019).
- [21] S. H. Lee, D. Graf, L. Min, Y. Zhu, H. Yi, S. Ciocys, Y. Wang, E. S. Choi, R. Basnet, A. Fereidouni, A. Wegner, Y.-F. Zhao, K. Verlinde, J. He, R. Redwing, V. Gopalan, H. O. H. Churchill, A. Lanzara, N. Samarth, C.-Z. Chang *et al.*, Evidence for a magnetic-field-induced ideal type-II Weyl state in antiferromagnetic topological insulator $\text{Mn}(\text{Bi}_{1-x}\text{Sb}_x)_2\text{Te}_4$, *Phys. Rev. X* **11**, 031032 (2021).
- [22] J. Li, Y. Li, S. Du, Z. Wang, B.-L. Gu, S.-C. Zhang, K. He, W. Duan, and Y. Xu, Intrinsic magnetic topological insulators in van der Waals layered MnBi_2Te_4 -family materials, *Sci. Adv.* **5**, eaaw5685 (2019).
- [23] Z. Li, J. Li, K. He, X. Wan, W. Duan, and Y. Xu, Tunable interlayer magnetism and band topology in van der Waals heterostructures of MnBi_2Te_4 -family materials, *Phys. Rev. B* **102**, 081107(R) (2020).
- [24] Y. Tokura, K. Yasuda, and A. Tsukazaki, Magnetic topological insulators, *Nat. Rev. Phys.* **1**, 126 (2020).
- [25] F. Hou, Q. Yao, C.-S. Zhou, X.-M. Ma, M. Han, Y. J. Hao, X. Wu, Y. Zhang, H. Sun, C. Liu, Y. Zhao, Q. Liu, and J. Lin, Te-vacancy-induced surface collapse and reconstruction in antiferromagnetic topological insulator MnBi_2Te_4 , *ACS Nano* **14**, 11262 (2020).
- [26] Y. Lai, L. Ke, J. Yan, R. D. McDonald, and R. J. McQueeney, Defect-driven ferrimagnetism and hidden magnetization in MnBi_2Te_4 , *Phys. Rev. B* **103**, 184429 (2021).
- [27] J.-Q. Yan, S. Okamoto, M. A. McGuire, A. F. May, R. J. McQueeney, and B. C. Sales, Evolution of structural, magnetic, and transport properties in $\text{MnBi}_{2-x}\text{Sb}_x\text{Te}_4$, *Phys. Rev. B* **100**, 104409 (2019).
- [28] P. Li, J. Yu, Y. Wang, and W. Luo, Electronic structures and topological phases of magnetic layered materials MnBi_2Te_4 , MnBi_2Se_4 and MnSb_2Te_4 , *Phys. Rev. B* **103**, 155118 (2021).
- [29] W. Ko, M. Kolmer, J. Yan, A. D. Pham, M. Fu, F. Lüpke, S. Okamoto, Z. Gai, P. Ganesh, and A.-P. Li, Realizing gapped surface states in the magnetic topological insulator $\text{MnBi}_{2-x}\text{Sb}_x\text{Te}_4$, *Phys. Rev. B* **102**, 115402 (2020).
- [30] S. X. M. Riberolles, Q. Zhang, E. Gordon, N. P. Butch, L. Ke, J.-Q. Yan, and R. J. McQueeney, Evolution of magnetic interactions in Sb-substituted MnBi_2Te_4 , *Phys. Rev. B* **104**, 064401 (2021).
- [31] S. Wimmer, J. SanchezBarriga, P. Kppers, A. Ney, E. Schierle, F. Freyse, O. Caha, J. Michalika, M. Liebmann, D. Primetzhofner, M. Hoffman, A. Ernst, M. M. Otrokov, G. Bihlmayer, E. Weschke, B. Lake, E. V. Chulkov, M. Morgenstern, G. Bauer, G. Springholz *et al.*, MnRich MnSb_2Te_4 : A topological insulator with magnetic gap closing at high Curie temperatures of 45-50 K, *Adv. Mater.* **33**, 2102935 (2021).
- [32] Y. Liu, L.-L. Wang, Q. Zheng, Z. Huang, X. Wang, M. Chi, Yan Wu, B. C. Chakoumakos, M. A. McGuire, B. C. Sales, W. Wu,

- and J. Yan, Site mixing for engineering magnetic topological insulators, *Phys. Rev. X* **11**, 021033 (2021).
- [33] S. V. Eremeev, I. P. Rusinov, Yu. M. Koroteev, A. Yu. Vyazovskaya, M. Hoffmann, P. M. Echenique, A. Ernst, M. M. Otrokov, and E. V. Chulkov, Topological magnetic materials of the $(\text{MnSb}_2\text{Te}_4) \cdot (\text{Sb}_2\text{Te}_3)_n$ van der Waals compounds family, *J. Phys. Chem. Lett.* **12**, 4268 (2021).
- [34] T. Murakami, Y. Nambu, T. Koretsune, Gu Xiangyu, T. Yamamoto, C. M. Brown, and H. Kageyama, Realization of interlayer ferromagnetic interaction in MnSb_2Te_4 toward the magnetic Weyl semimetal state, *Phys. Rev. B* **100**, 195103 (2019).
- [35] B. Xu, Y. Zhang, E. H. Alizade, Z. A. Jahangirli, F. Lyzwa, E. Sheveleva, P. Marsik, Y. K. Li, Y. G. Yao, Z. W. Wang, B. Shen, Y. M. Dai, V. Kataev, M. M. Otrokov, E. V. Chulkov, N. T. Mamedov, and C. Bernhard, Infrared study of the multi-band low-energy excitations of the topological antiferromagnet MnBi_2Te_4 , *Phys. Rev. B* **103**, L121103 (2021).
- [36] M. Köpf, J. Ebad-Allah, S. H. Lee, Z. Q. Mao, and C. A. Kuntscher, Influence of magnetic ordering on the optical response of the antiferromagnetic topological insulator MnBi_2Te_4 , *Phys. Rev. B* **102**, 165139 (2020).
- [37] M. Köpf, S. H. Lee, H. Kumar, Z. Q. Mao, and C. A. Kuntscher, Infrared study of the layered magnetic insulator $\text{Mn}(\text{Bi}_{0.07}\text{Sb}_{0.93})_2\text{Te}_4$ at low temperatures, *Phys. Rev. B* **105**, 195125 (2022).
- [38] M. Köpf, S. H. Lee, Z. Q. Mao, and C. A. Kuntscher, Evolution of the optical response of the magnetic topological insulators $\text{Mn}(\text{Bi}_{1-x}\text{Sb}_x)_2\text{Te}_4$ with Sb content, *Phys. Rev. B* **106**, 195118 (2022).
- [39] C. Pei, Y. Xia, J. Wu, Y. Zhao, L. Gao, T. Ying, B. Gao, N. Li, W. Yang, D. Zhang, H. Gou, Y. Chen, H. Hosono, G. Li, and Y. Qi, Pressure-induced topological and structural phase transitions in an antiferromagnetic topological insulator, *Chin. Phys. Lett.* **37**, 066401 (2020).
- [40] W.-T. Guo, L. Huang, Y. Yang, Z. Huang, and J.-M. Zhang, Pressure-induced topological quantum phase transition in the magnetic topological insulator MnBi_2Te_4 , *New J. Phys.* **23**, 083030 (2021).
- [41] K. Y. Chen, B. S. Wang, J.-Q. Yan, D. S. Parker, J.-S. Zhou, Y. Uwatoko, and J.-G. Cheng, Suppression of the antiferromagnetic metallic state in the pressurized MnBi_2Te_4 single crystal, *Phys. Rev. Mat.* **3**, 094201 (2019).
- [42] Z. Xu, M. Ye, J. Li, W. Duan, and Y. Xu, Hydrostatic pressure-induced magnetic and topological phase transitions in the MnBi_2Te_4 family of materials, *Phys. Rev. B* **105**, 085129 (2022).
- [43] J. Shao, Y. Liu, M. Zeng, J. Li, X. Wu, X.-M. Ma, F. Jin, R. Lu, Y. Sun, M. Gu, K. Wang, W. Wu, L. Wu, C. Liu, Q. Liu, and Y. Zhao, Pressure-tuned intralayer exchange in superlattice-like $\text{MnBi}_2\text{Te}_4/(\text{Bi}_2\text{Te}_3)_n$ topological insulators, *Nano Lett.* **21**, 5874 (2021).
- [44] S. K. Chong, C. Lei, J. Li, Y. Cheng, D. Graf, S. H. Lee, M. Tanabe, T.-H. Yang, Z. Mao, A. H. MacDonald, and K. L. Wang, Pressure tunable quantum anomalous Hall states in a topological antiferromagnet, [arXiv:2306.10325](https://arxiv.org/abs/2306.10325).
- [45] R. M. Hazen, High-pressure phenomena, *Encyclopedia Britannica* (2009), <https://www.britannica.com/science/high-pressure-phenomena>.
- [46] K. Matsubayashi, T. Terai, J. S. Zhou, and Y. Uwatoko, Superconductivity in the topological insulator Bi_2Te_3 under hydrostatic pressure, *Phys. Rev. B* **90**, 125126 (2014).
- [47] Y. Yin, X. Ma, D. Yan, C. Yi, B. Yue, J. Dai, L. Zhao, X. Yu, Y. Shi, J.-T. Wang, and F. Hong, Pressure-driven electronic and structural phase transition in intrinsic magnetic topological insulator MnSb_2Te_4 , *Phys. Rev. B* **104**, 174114 (2021).
- [48] J. Wilks and E. Wilks, *Properties and Application of Diamond* (Butterworth-Heinemann Ltd., Oxford, 1991).
- [49] D. B. Tanner, Use of x-ray scattering functions in Kramers-Kronig analysis of reflectance, *Phys. Rev. B* **91**, 035123 (2015).
- [50] A. B. Kuzmenko, Kramers-Kronig constrained variational analysis of optical spectra, *Rev. of Sci. Instrum.* **76**, 083108 (2005).
- [51] I. M. Lifshitz, Anomalies of electron characteristics of a metal in the high pressure region, *JETP* **11**, 1130 (1960).
- [52] A. Polian, M. Gauthier, S. M. Souza, D. M. Triches, J. C. de Lima, and T. A. Grandi, Two-dimensional pressure-induced electronic topological transition in Bi_2Te_3 , *Phys. Rev. B* **83**, 113106 (2011).
- [53] O. Gomis, R. Vilaplana, F. J. Manjon, P. Rodriguez-Hernandez, E. Perez-Gonzalez, A. Munoz, V. Kucek, and C. Drasar, Lattice dynamics of Sb_2Te_3 at high pressures, *Phys. Rev. B* **84**, 174305 (2011).
- [54] R. Vilaplana, D. Santamaría-Pérez, O. Gomis, F. J. Manjón, J. González, A. Segura, A. Muñoz, P. Rodríguez-Hernández, E. Pérez-González, V. Marín-Borrás, V. Muñoz-Sanjose, C. Drasar, and V. Kucek, Structural and vibrational study of Bi_2Se_3 under high pressure, *Phys. Rev. B* **84**, 184110 (2011).
- [55] R. Vilaplana, O. Gomis, F. J. Manjon, A. Segura, E. Perez-Gonzalez, P. Rodriguez-Hernandez, A. Munoz, J. Gonzalez, V. Marin-Borras, V. Munoz-Sanjose, C. Drasar, and V. Kucek, High-pressure vibrational and optical study of Bi_2Te_3 , *Phys. Rev. B* **84**, 104112 (2011).
- [56] M. Bahramy, B. J. Yand, R. Arita, and N. Nagaosa, Emergence of non-centrosymmetric topological insulating phase in BiTeI under pressure, *Nat. Commun.* **3**, 679 (2012).
- [57] X. Xi, C. Ma, Z. Liu, Z. Chen, W. Ku, H. Berger, C. Martin, D. B. Tanner, and G. L. Carr, Signatures of a pressure-induced topological quantum phase transition in BiTeI , *Phys. Rev. Lett.* **111**, 155701 (2013).
- [58] Z. Zhu, Y. Cheng, and U. Schwingenschlögl, Topological phase transition in layered GaS and GaSe , *Phys. Rev. Lett.* **108**, 266805 (2012).
- [59] M. Yang, Y. Z. Luo, M. G. Zeng, L. Shen, Y. H. Lu, J. Zhou, S. J. Wang, I. K. Sou, and Y. P. Feng, Pressure induced topological phase transition in layered Bi_2S_3 , *Phys. Chem. Chem. Phys.* **19**, 29372 (2017).
- [60] D. Bassanezi, E. O. Wrasse, and T. M. Schmidt, Symmetry-dependent topological phase transitions in PbTe layers, *Mater. Res. Express* **5**, 015051 (2018).
- [61] A. Ohmura, Y. Higuchi, T. Ochiai, M. Kanou, F. Ishikawa, S. Nakano, A. Nakayama, Y. Yamada, and T. Sasagawa, Pressure-induced topological phase transition in the polar semiconductor BiTeBr , *Phys. Rev. B* **95**, 125203 (2017).
- [62] V. Rajaji, U. Dutta, P. C. Sreeparvathy, S. Ch. Sarma, Y. A. Sorb, B. Joseph, S. Sahoo, S. C. Peter, V. Kanchana, and C. Narayana, Structural, vibrational, and electrical properties of $1T\text{-TiTe}_2$ under hydrostatic pressure: Experiments and theory, *Phys. Rev. B* **97**, 085107 (2018).

- [63] J. Ebad-Allah, M. Krottenmüller, J. Hu, Y. L. Zhu, Z. Q. Mao, and C. A. Kuntscher, Infrared spectroscopy study of the nodal-line semimetal candidate ZrSiTe under pressure: Hints for pressure-induced phase transitions, *Phys. Rev. B* **99**, 245133 (2019).
- [64] M. Krottenmüller, M. Vöst, N. Unglert, J. Ebad-Allah, G. Eickerling, D. Volkmer, J. Hu, Y. L. Zhu, Z. Q. Mao, W. Scherer, and C. A. Kuntscher, Indications for Lifshitz transitions in the nodal-line semimetal ZrSiTe induced by interlayer interaction, *Phys. Rev. B* **101**, 081108(R) (2020).
- [65] T. Qian, Y.-T. Yao, C. Hu, E. Feng, H. Cao, I. I. Mazin, T.-R. Chang, and N. Ni, Magnetic dilution effect and topological phase transitions in $(\text{Mn}_{1-x}\text{Pb}_x)\text{Bi}_2\text{Te}_4$, *Phys. Rev. B* **106**, 045121 (2022).
- [66] L. Zhou, Z. Tan, D. Yan, Z. Fang, Y. Shi, and H. Weng, Topological phase transition in the layered magnetic compound MnSb_2Te_4 : Spin-orbit coupling and interlayer coupling dependence, *Phys. Rev. B* **102**, 085114 (2020).
- [67] P. Y. Yu and M. Cardona, *Fundamentals of Semiconductors* (Springer, Heidelberg, 2010), pp. 203–205.
- [68] F. Wooten, *Optical Properties of Solids* (Academic Press, New York, 1972), pp. 85–90.
- [69] M. Fox, *Optical Properties of Solids* (Oxford University Press, New York, 2001), pp. 143–145.
- [70] Q. D. Gibson, H. Wu, T. Liang, M. N. Ali, N. P. Ong, Q. Huang, and R. J. Cava, Magnetic and electronic properties of CaMn_2Bi_2 : A possible hybridization gap semiconductor, *Phys. Rev. B* **91**, 085128 (2015).
- [71] C. Lane, M. M. Piva, P. F. S. Rosa, and X.-Z. Zhu, Correlation versus hybridization gap in CaMn_2Bi_2 , *Sci. Rep.* **13**, 9271 (2023).
- [72] M. M. Piva, S. M. Thomas, Z. Fisk, J.-X. Zhu, J. D. Thompson, P. G. Pagliuso, and P. F. S. Rosa, Putative hybridization gap in CaMn_2Bi_2 under applied pressure, *Phys. Rev. B* **100**, 045108 (2019).